Supplementary Information for: Constraints on the behaviour and content of volatiles in Galápagos magmas from melt inclusions and nominally anhydrous minerals

Matthew L. M. Gleeson[1,2]*, Sally A. Gibson[2], Michael J. Stock[3], and EIMF[4]

[1]School of Earth and Environmental Sciences, Cardiff University, Main Building, Park Place, Cardiff, CF10 3AT, UK.

[2]Department of Earth Sciences, University of Cambridge, Downing Street, Cambridge, CB2 3EQ, UK.

[3]Department of Geology, Trinity College Dublin, College Green, Dublin 2, Ireland.

[4]Edinburgh Ion Microprobe Facility, University of Edinburgh, Grant Institute, School of Geosciences, Edinburgh, EH9 3JW, UK.

Corresponding author email address: gleesonm1@cardiff.ac.uk

SIMS CALIBRATION DATA

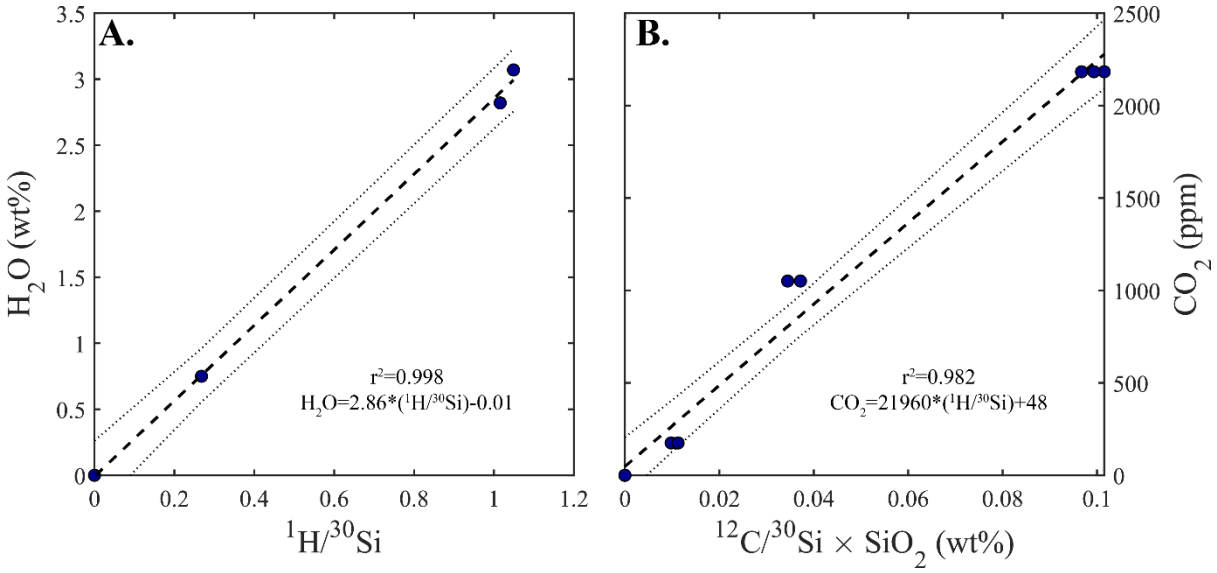

Figure S.1 – *Calibration data for H_2O and CO_2 analysis in the melt inclusions, embayments and matrix glasses. Calibration data taken from Shishkina et al. (2010).*

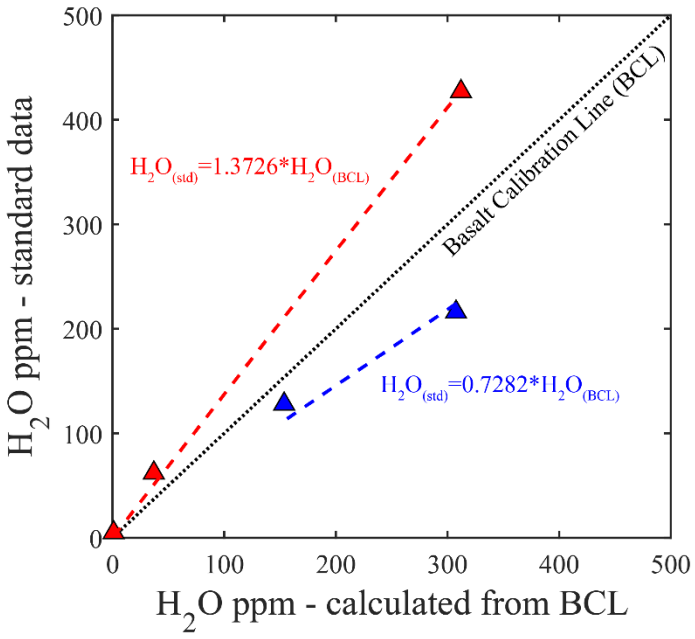

Figure S.2 – *Calibration data for Nominally Anhydrous Minerals (NAMs). Determination of NAM H_2O contents from a calibration line constructed from analyses of basaltic glasses (as shown in Fig S.1) leads to the H_2O concentration of clinopyroxene and orthopyroxenes being underpredicted and overpredicted, respectively. Matrix matched standards are therefore used to constrain the 'correction factors' as shown here. Calibration data are from Kumamoto et al. (2017).*

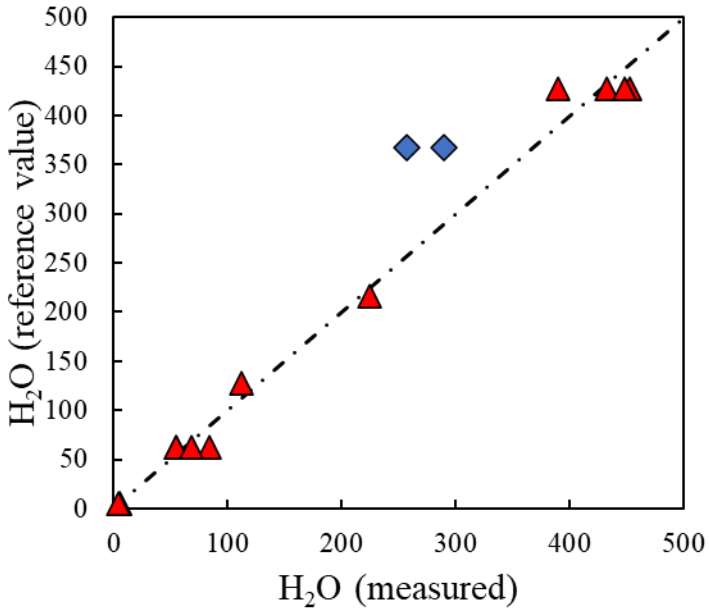

Figure S.3 – *Measured vs preferred results for all pyroxene standard data (including analyses involved in the calibration slope). Nearly all pyroxene analyses plot along a 1:1 line (red triangles). Analyses of the standard CPX-KH03-27 are also shown (blue diamonds). These two analyses of CPX-KH03-27 returned lower H_2O contents then their published values. We note, however, that the grain analysed in this study contains a much lower Al content than the published value, indicating some heterogeneity. Calibration data from Kumamoto et al. (2017).*

OLIVINE – MELT DISEQUILIBRIUM

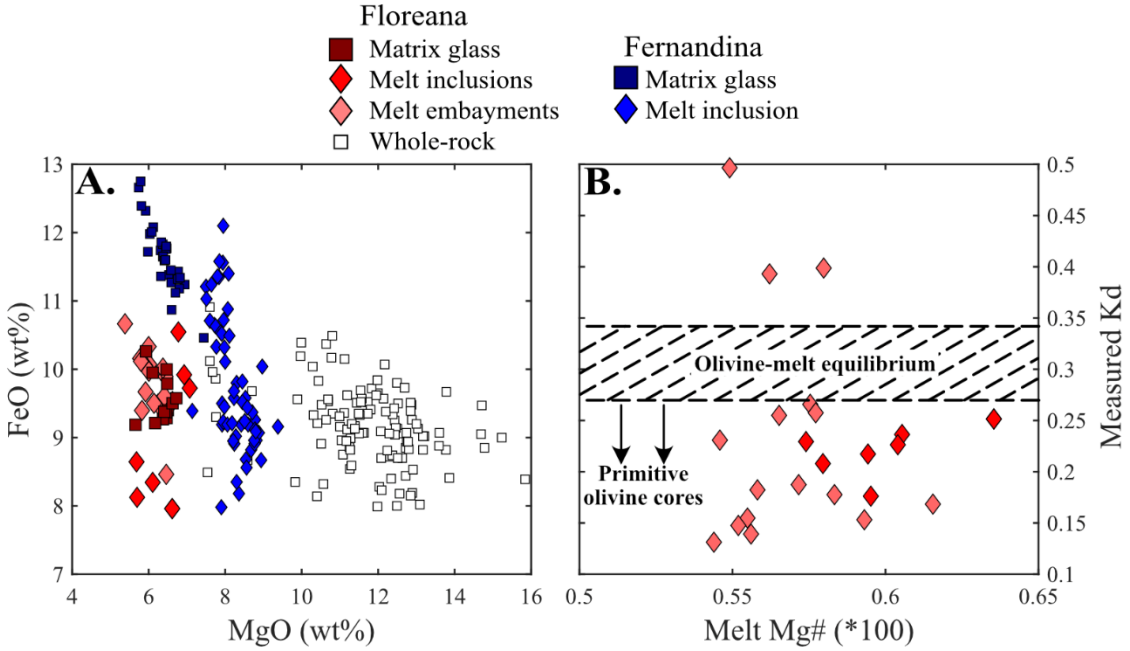

Figure S.4 – *FeO contents and olivine-melt disequilibrium in the Floreana melt inclusions and embayments.* ***A.*** *the range of FeO contents in the melt inclusions and embayments from Floreana olivines is similar to that observed in Floreana whole-rock analyses (Harpp et al. 2014). Some melt inclusions display moderately low FeO contents compared to the matrix glass of sample 17MMSG16, possibly indicating that limited FeO loss has occurred.* ***B.*** *The measured* $Kd_{melt\text{-}olivine}^{Fe\text{-}Mg}$ *between each melt inclusion/embayment is shown against the Mg# of the melt (all ratios calculated assuming an* Fe^{2+}/Fe_{tot} *ratio of 0.85). Most melt inclusions and embayments lie below the black dashed region, which represents the equilibrium values of Kd determined through experimental analysis (e.g. Matzen et al. 2011), indicating that the olivine hosts are more primitive than their trapped melts.*

MINIMUM ENTRAPMENT PRESSURES

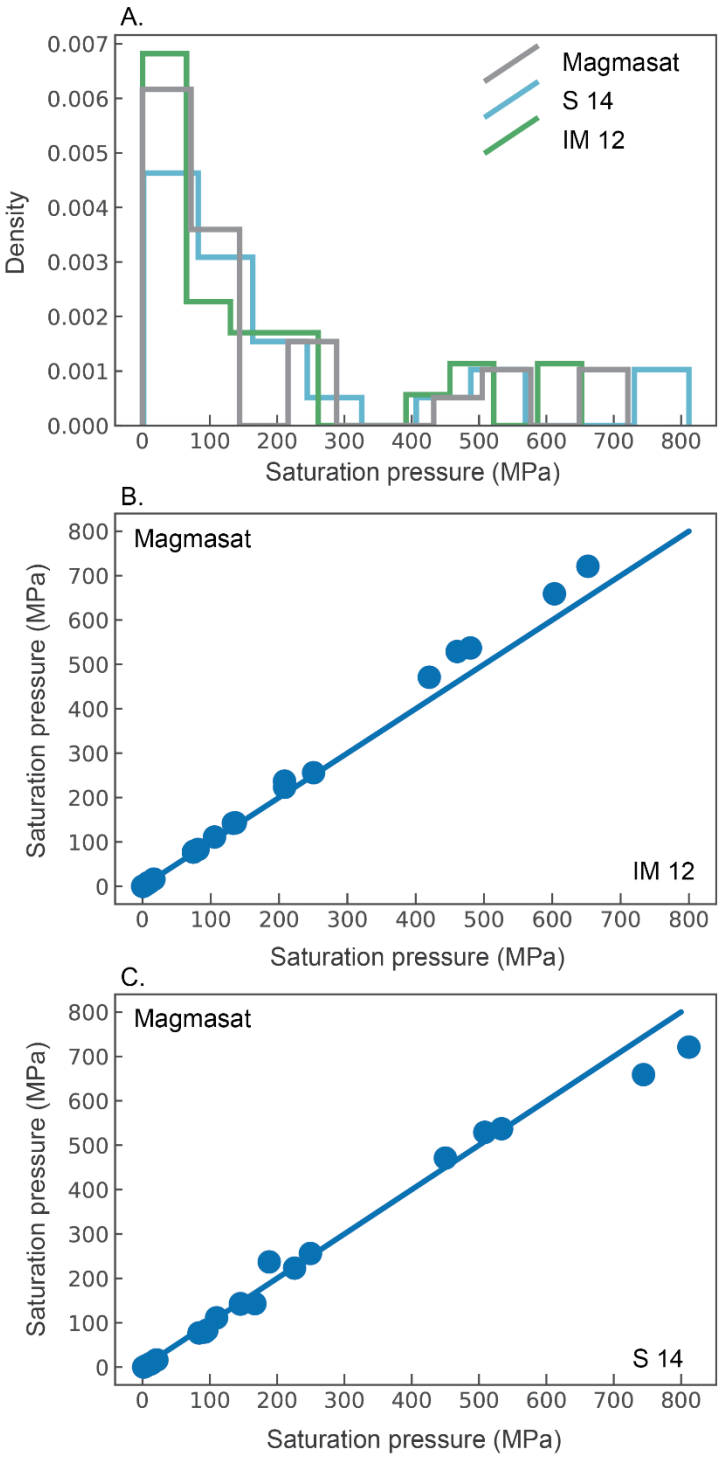

Figure S.5 – *Results of saturation calculations carried out in VESIcal (Iacovino et al., 2020).* ***A.*** *Histogram of saturation pressures from three different saturation models: Magmasat (Ghiorso and Gualda 2015); S 14 (Shishkina et al. 2014); and IM 12 (Iacono-Marziano et al. 2012).* ***B.*** *Comparison of results from Magmasat and IM 12. There is generally a very strong agreement between the two models, with slightly higher pressure predicted for the high CO_2 melt inclusions in Magmasat.* ***C.*** *Comparison of the results from Magmasat and S 14. There is a strong agreement between the two models, excluding the two samples that plot above the calibration range for Shishkina et al. (2014).*

VOLATILE DIFFUSION

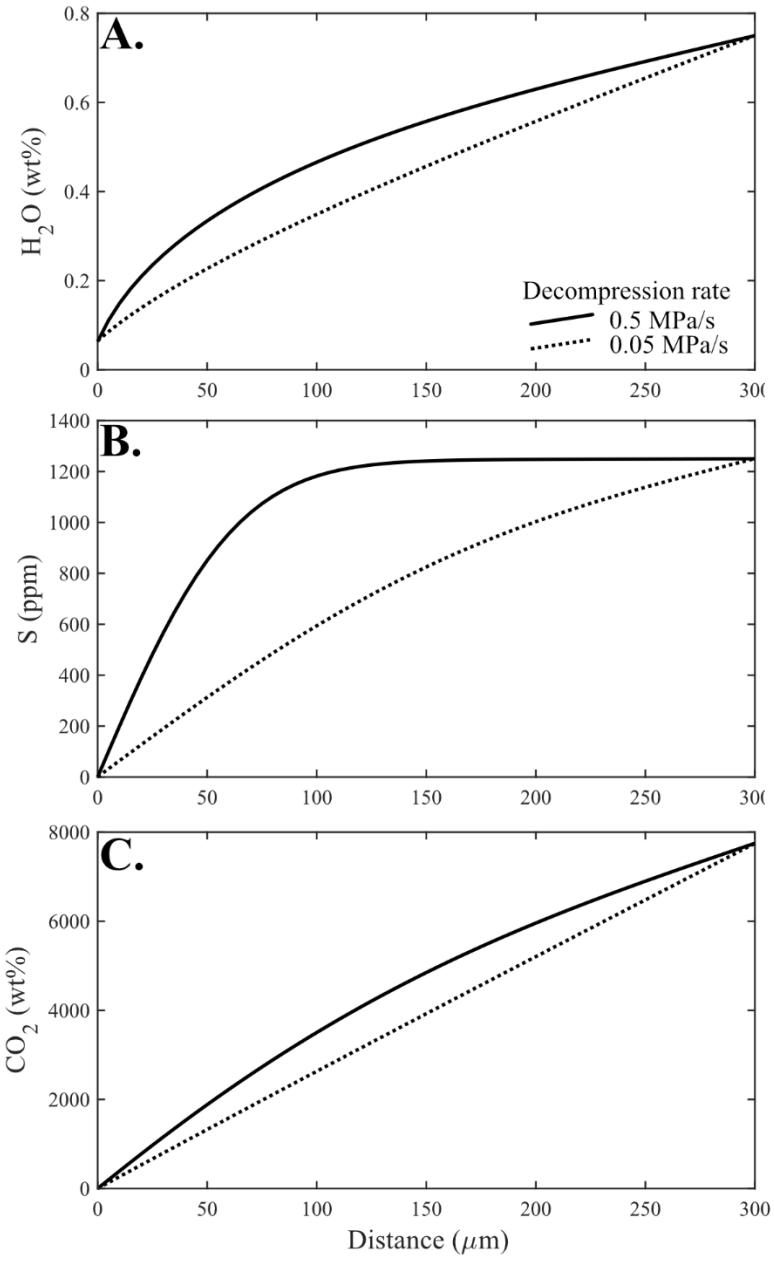

Figure S.6 – *Volatile contents contained within a hypothetical melt embayment following magma decompression and subsequent volatile loss via diffusion. Results are displayed for a 300µm embayment and decompression rates of 0.5 and 0.05 MPa/s. In both models shown here decompression initiates from a pressure of 750 MPa and the initial volatile content of the embayment is set at 0.75 wt% H_2O, 1250 ppm S, and 7750 ppm CO_2. Closed system degassing is assumed and no vapour phase is present in the system when the model initiates. Volatile solubility models are taken from Ghiorso and Gualda (2015) and Witham et al. (2012). Diffusivities are taken from Zhang and Ni (2010) and Zhang et al. (2010).*

SEM IMAGES

Backscatter electron images of all melt inclusions, melt embayments and pyroxenes that were analysed in this study are presented below. Each image shows where the analyses were taken and what H_2O and CO_2 contents were measured.

MELT INCLUSIONS AND MELT EMBAYMENTS

Mount mi2, olivine 39

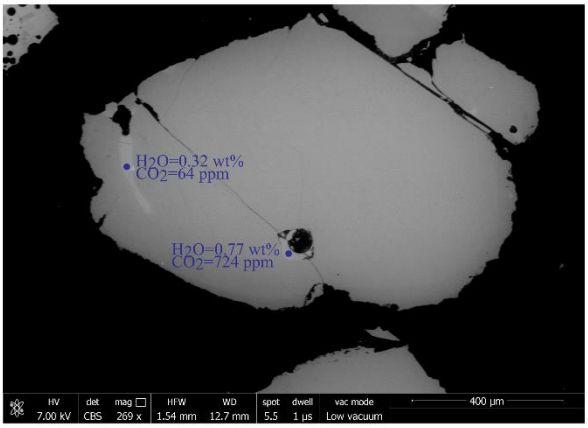

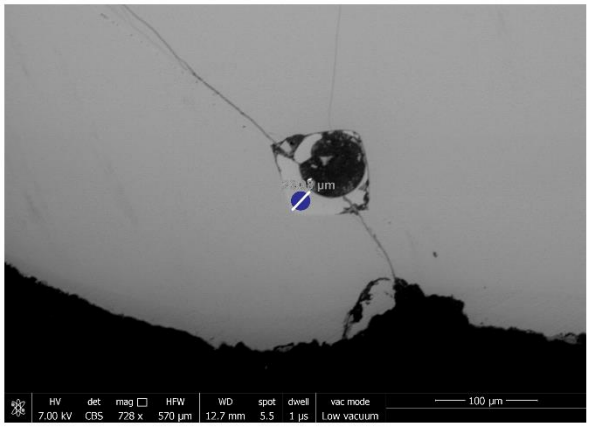

Mount mi2, olivine 9

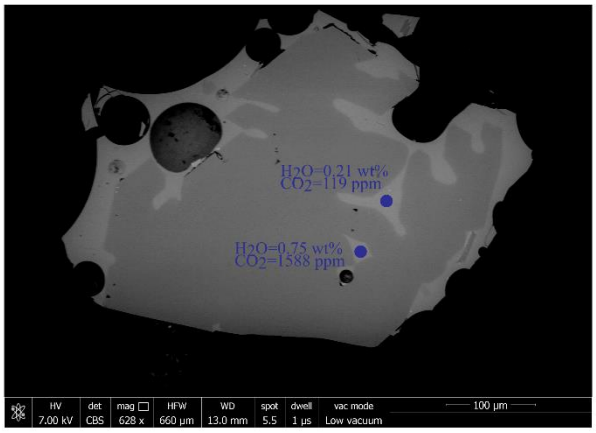

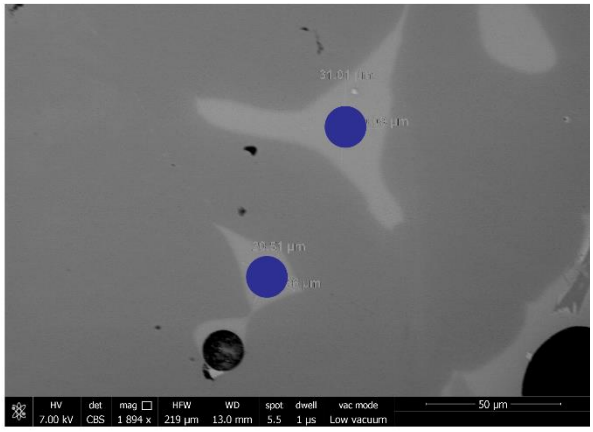

Mount mi2, olivine 8

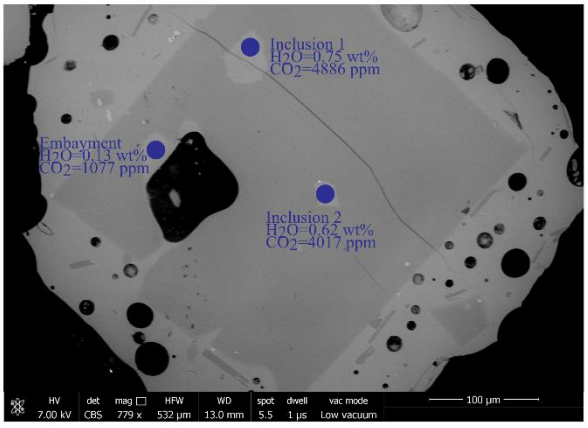

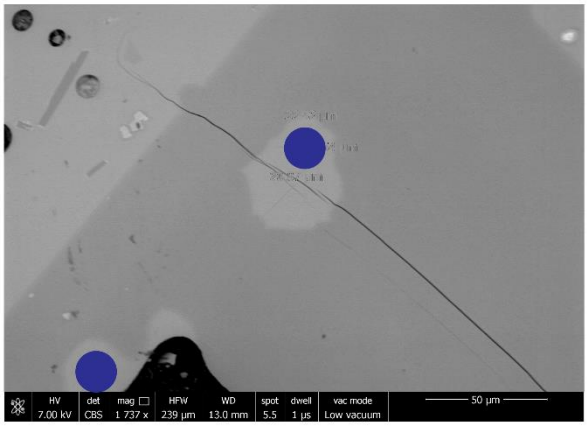

Mount m1, olivine 23 (additional polish applied prior to final analysis)

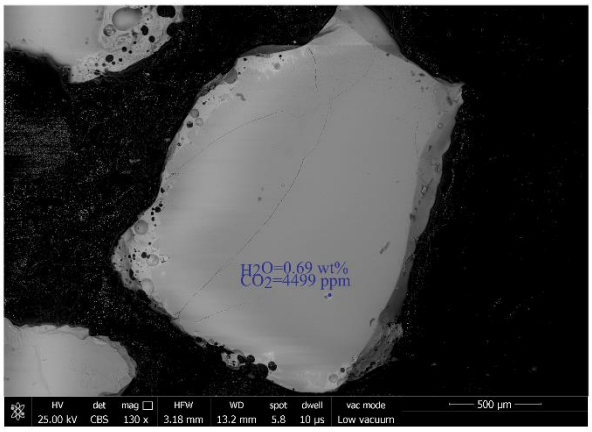

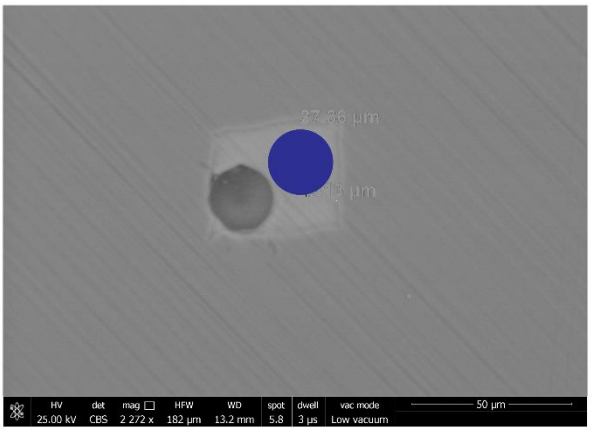

Mount m1, olivine 110

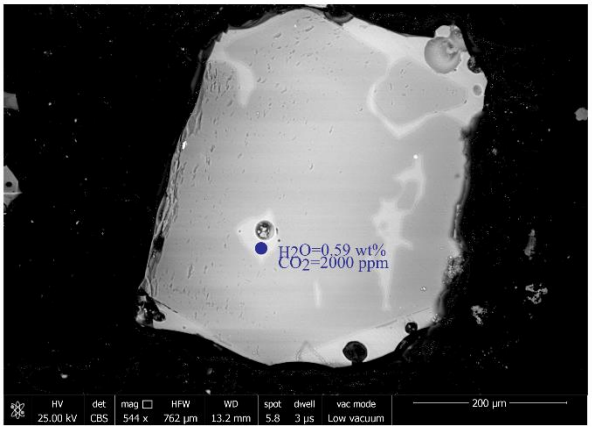

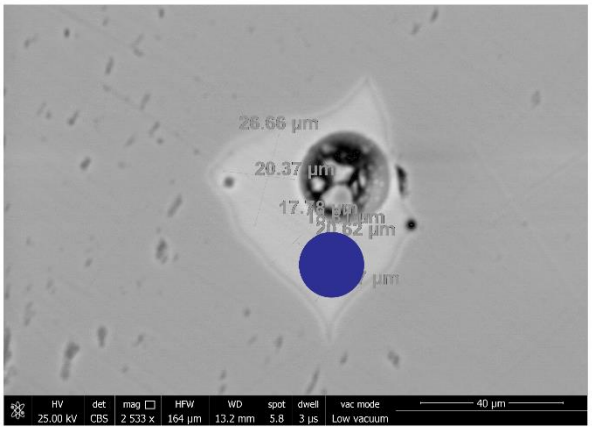

Mount m1, olivine 142 (elongate inclusion contained within broken crystal)

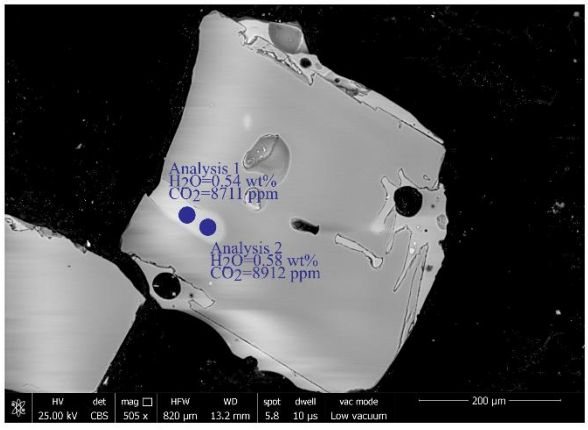

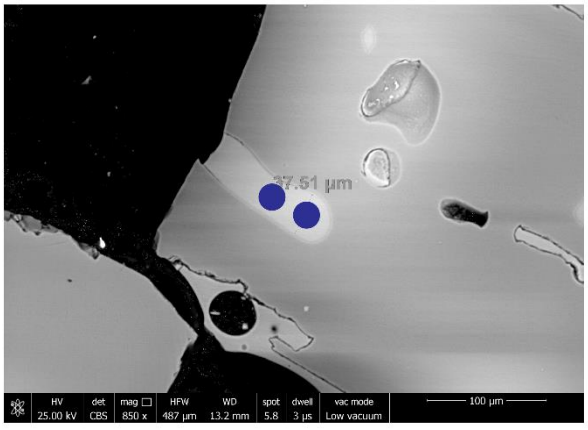

Mount m1, olivine 131 (embayment connected outside the plane of view)

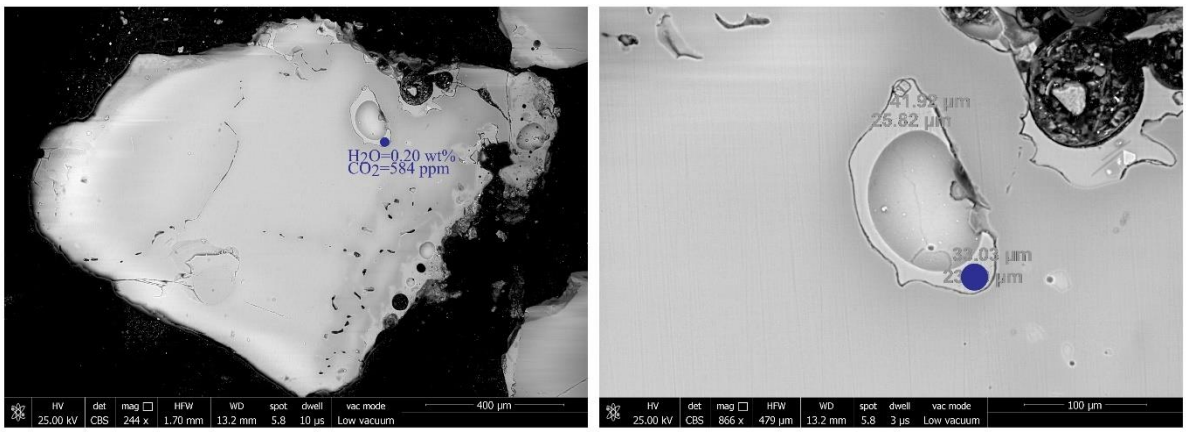

Mount m1, olivine 108 (embayment connected outside plane of view)

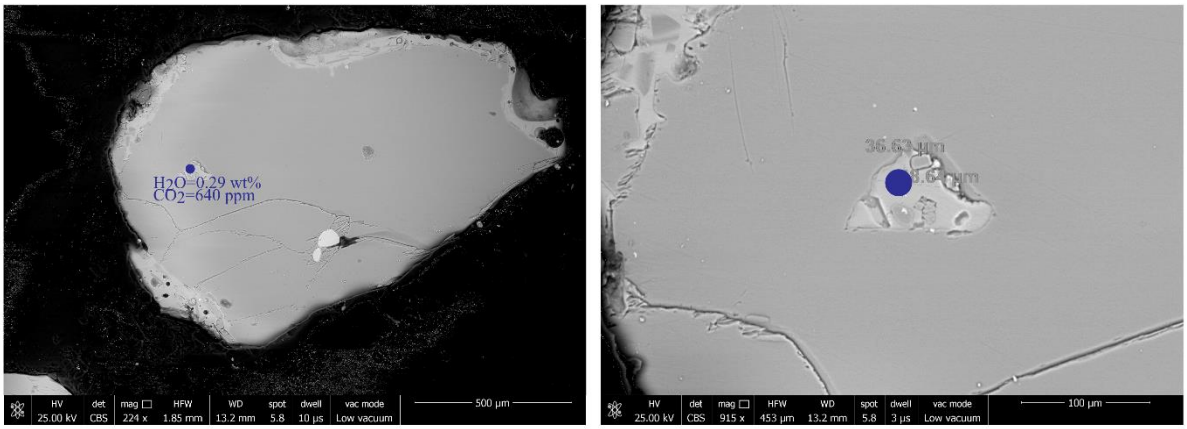

Mount mi2, olivine 38 (embayment connected outside plane of view)

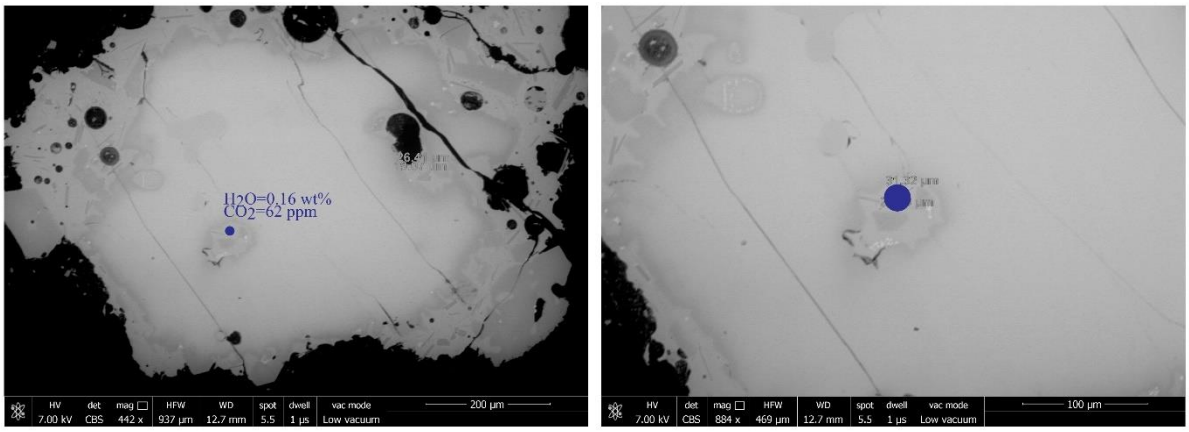

Mount mi2, olivine 24

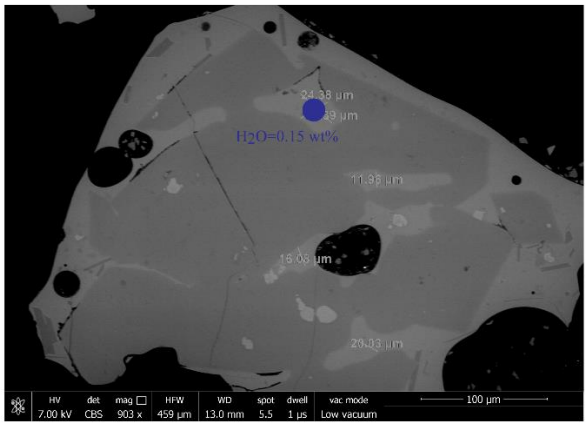

Mount mi2, olivine 21

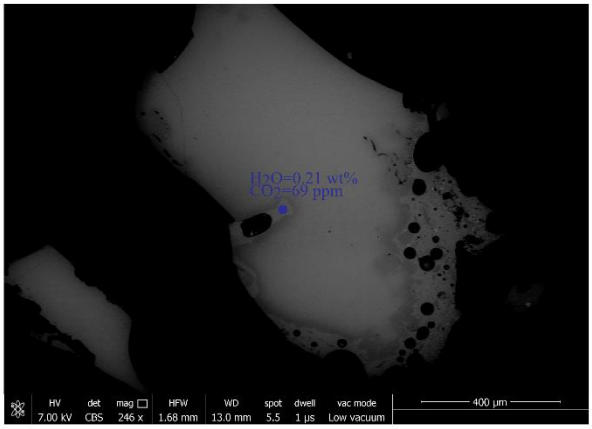

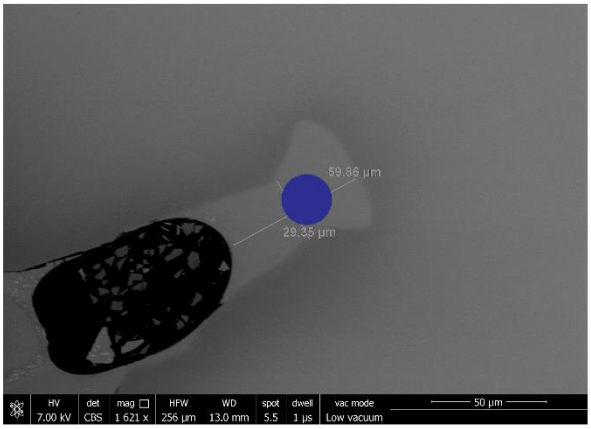

Mount mi2, olivine 15

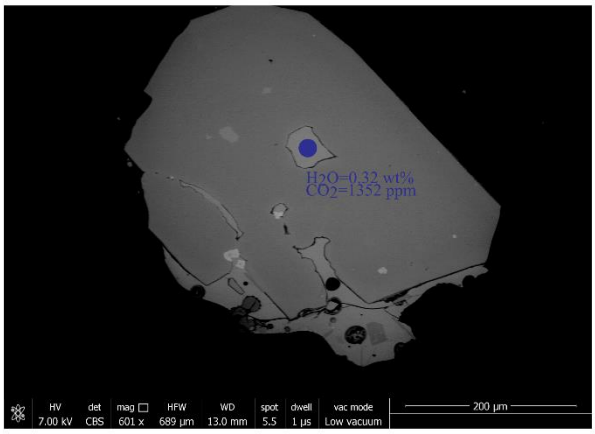

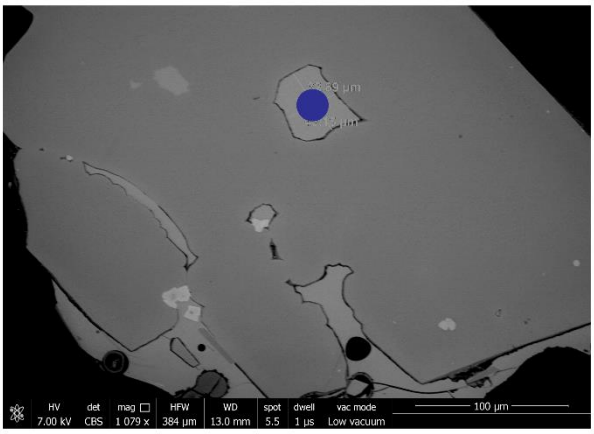

Mount mi2, olivine 16

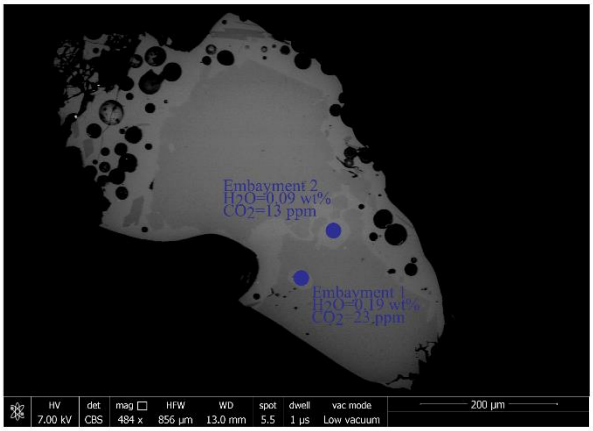

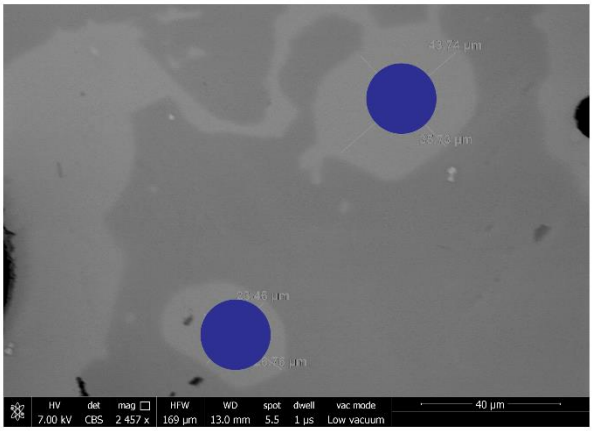

Mount mi1, olivine 18 (trapped melt pocket)

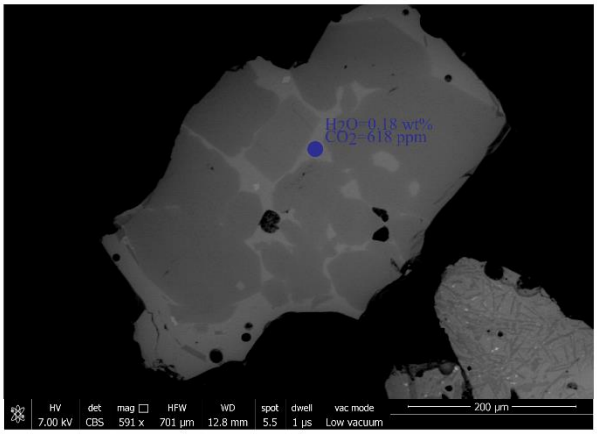

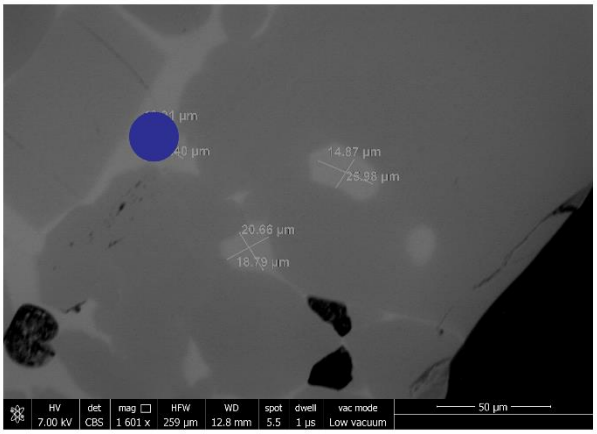

Mount mi1, olivine 23

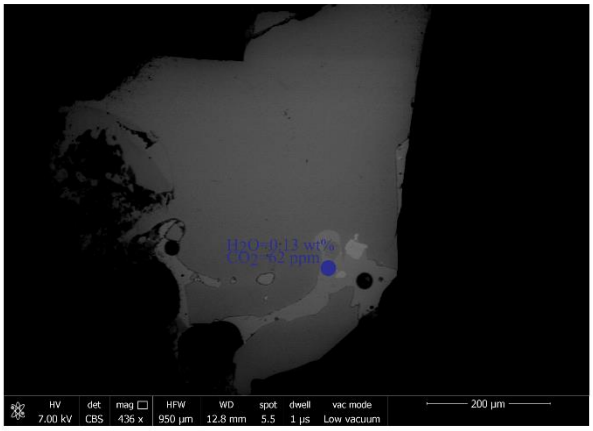

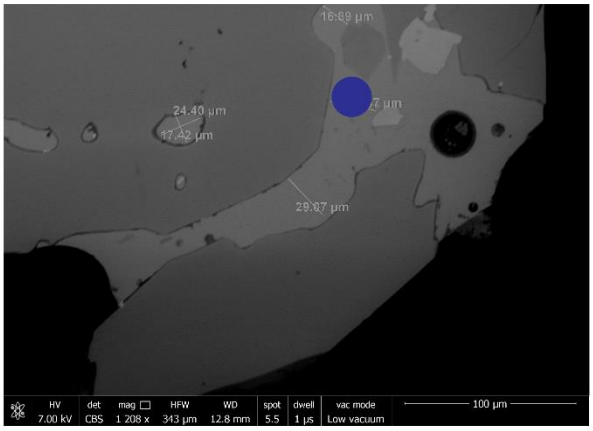

Mount m2, olivine 1

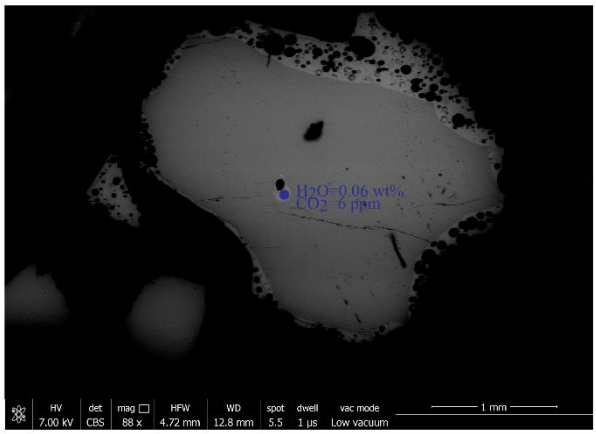

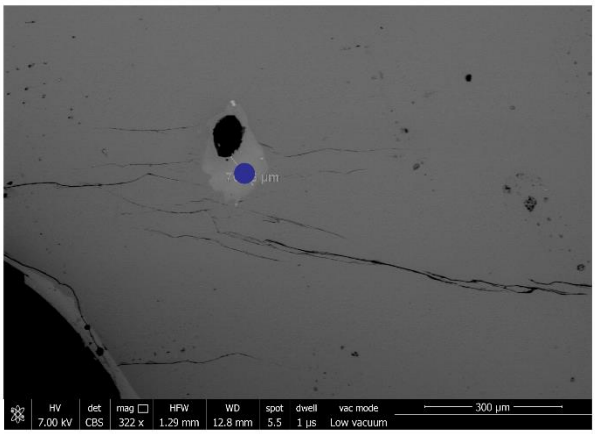

Mount m1, olivine 1

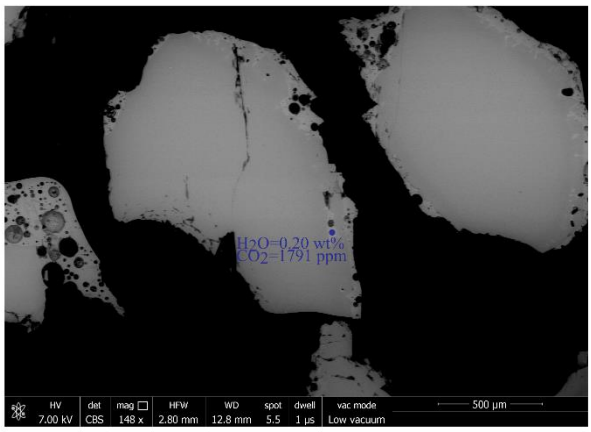

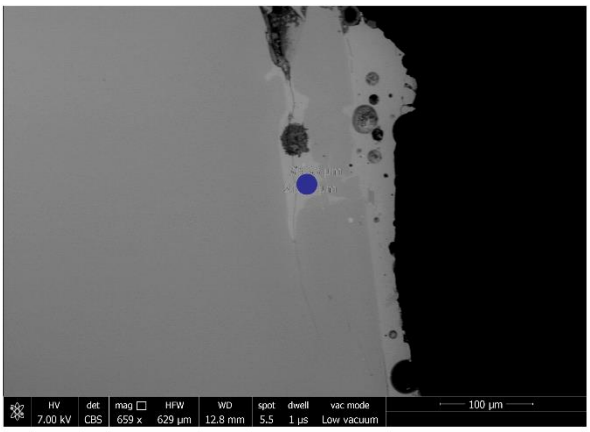

Mount m1, olivine 2

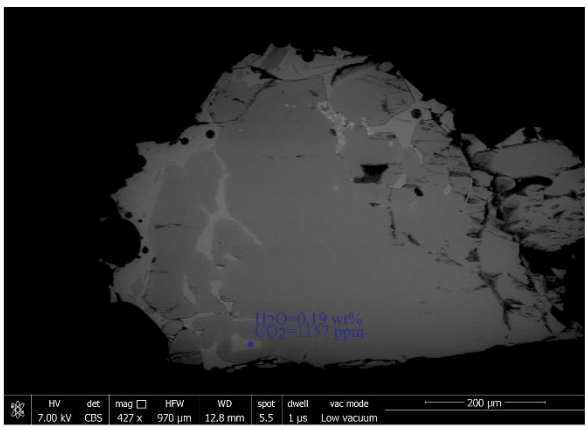

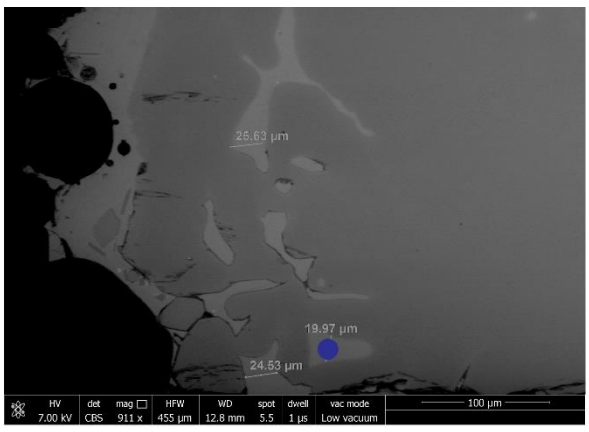

PYROXENE IMAGES

Sample 17MMSG16, pyroxene 3

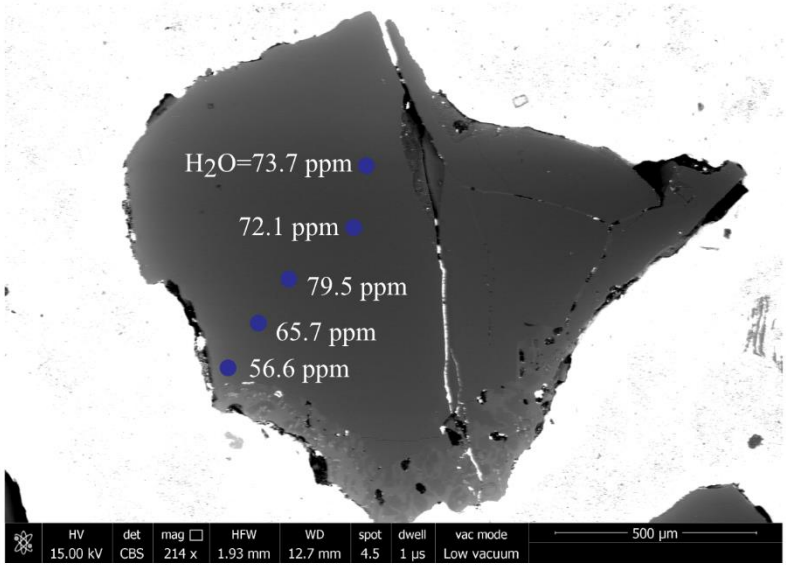

Sample 17MMSG16, pyroxene 4

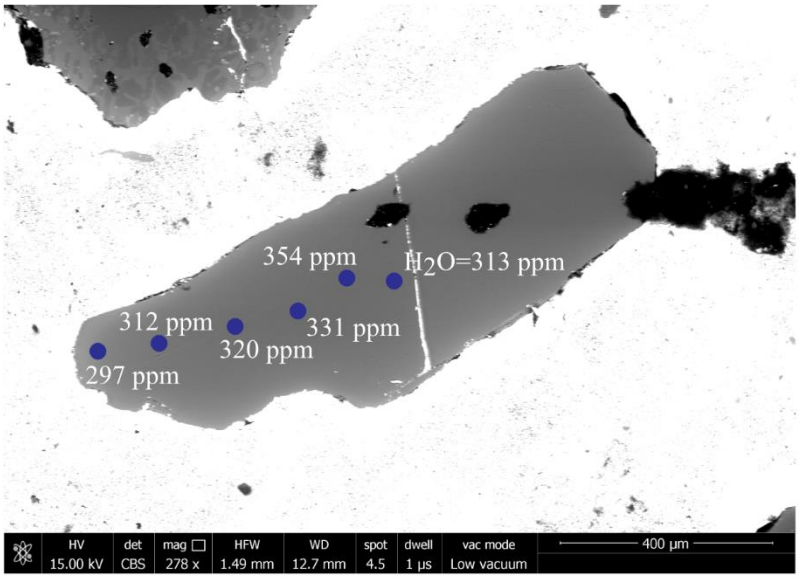

Sample 17MMSG16, pyroxene 5

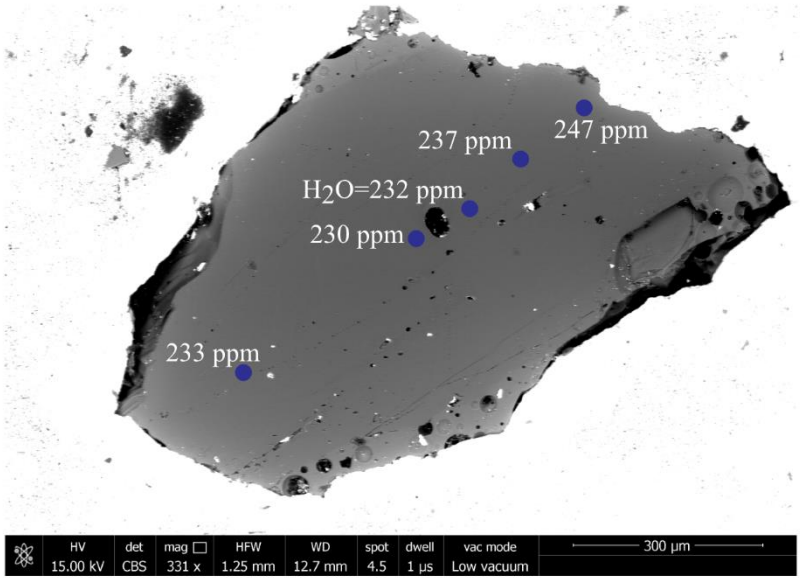

Sample 17MMSG16, pyroxene 7

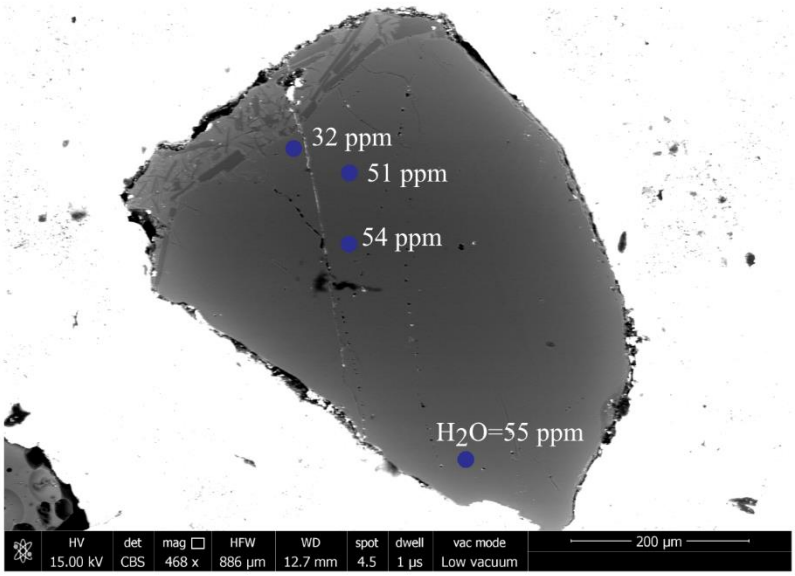

Sample 17MMSG16, pyroxene 8 (late stage rehydration of a low level/degassed pyroxene crystal?)

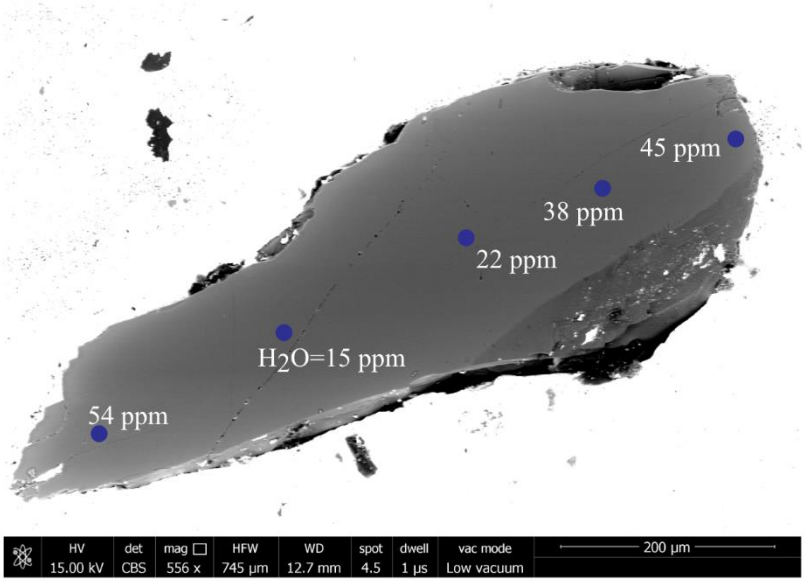

Sample 17MMSG16, pyroxene 9

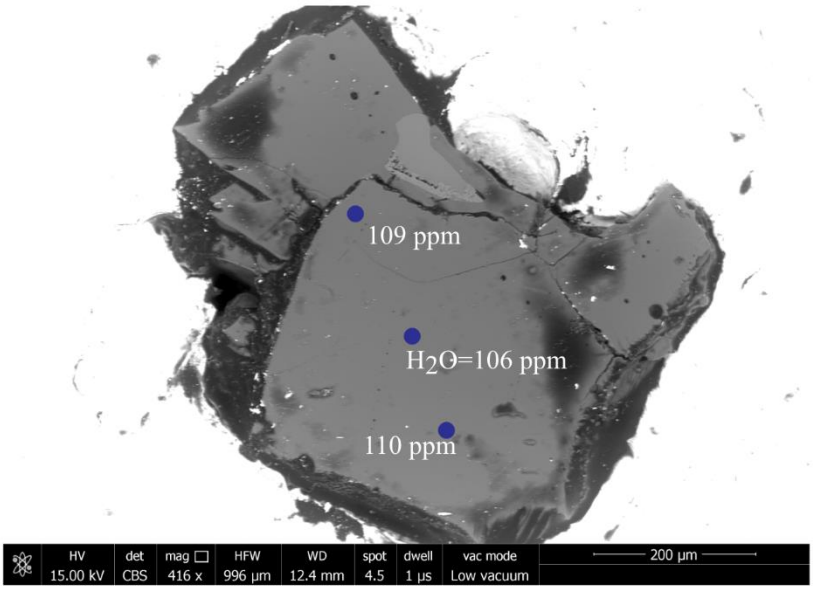

All pyroxenes from sample 17MMSG20 contain H_2O contents <<45 ppm and are interpreted to have lost H_2O via diffusion during ascent and/or cooling at the surface. 17MMSG20 represents a large scoria bomb (~10 cm diameter) and the matrix is notably more crystalline than that or the scoria fragments of 17MMSG16 (indicating a slower cooling rate).

Sample 17MMSG20, pyroxene 1

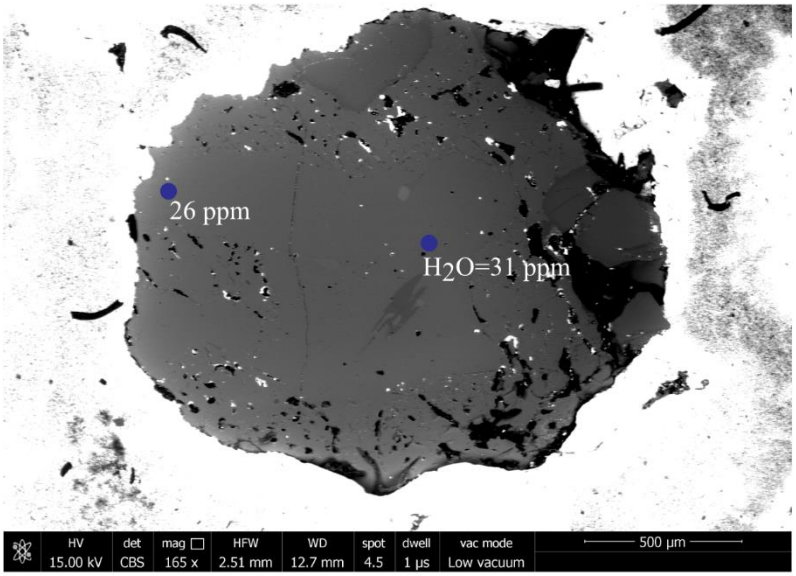

Sample 17MMSG20, pyroxene 2

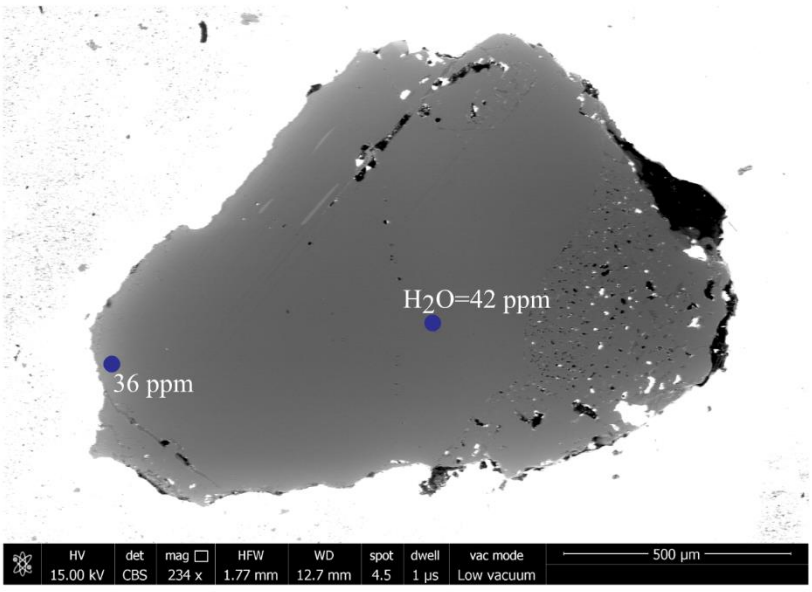

Sample 17MMSG20, pyroxene 3

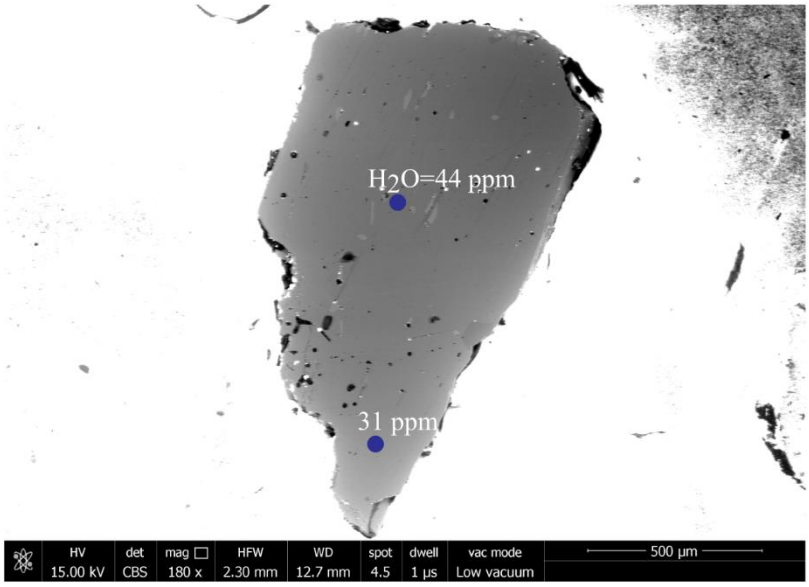

Sample 17MMSG20, pyroxene 5

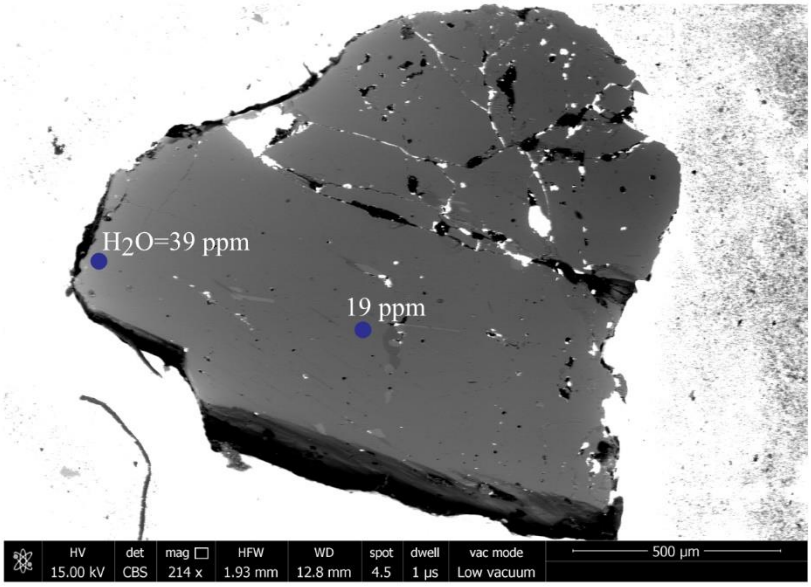

Sample 17MMSG20, pyroxene 6

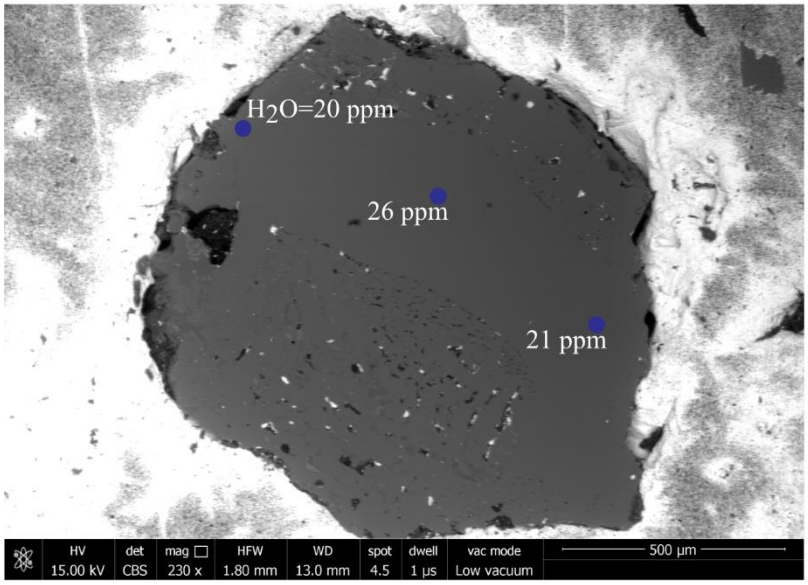

Sample 17MMSG20, pyroxene 7

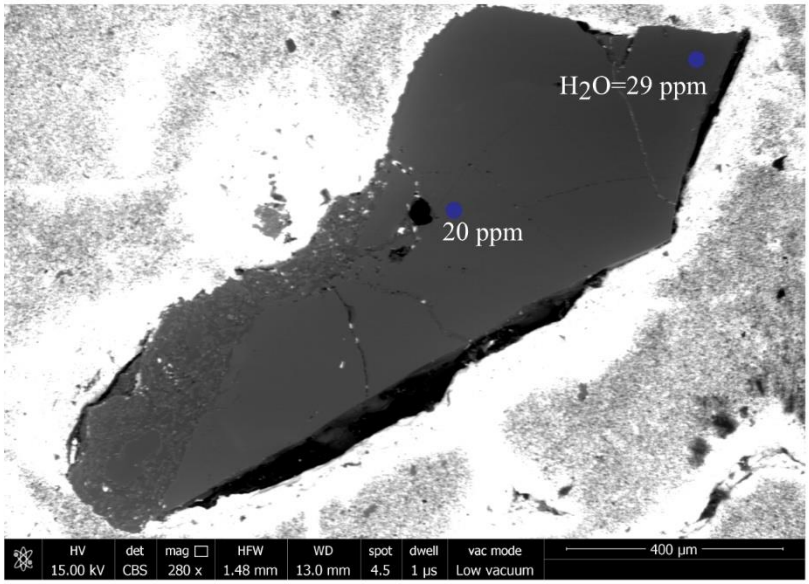

Sample 17MMSG20, pyroxene 8

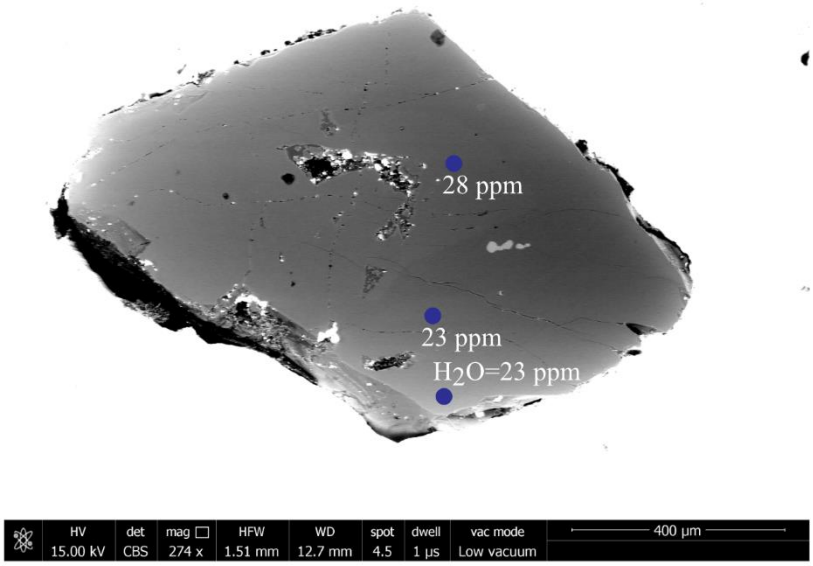

Clinopyroxenes from Floreana xenoliths

Sample 17MMSG02b, pyroxene 1

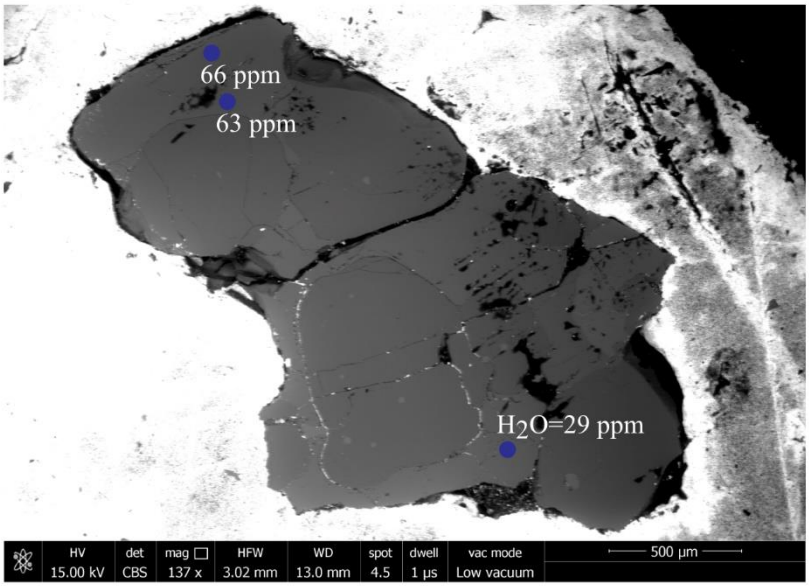

Sample 17MMSG02b, pyroxene 2

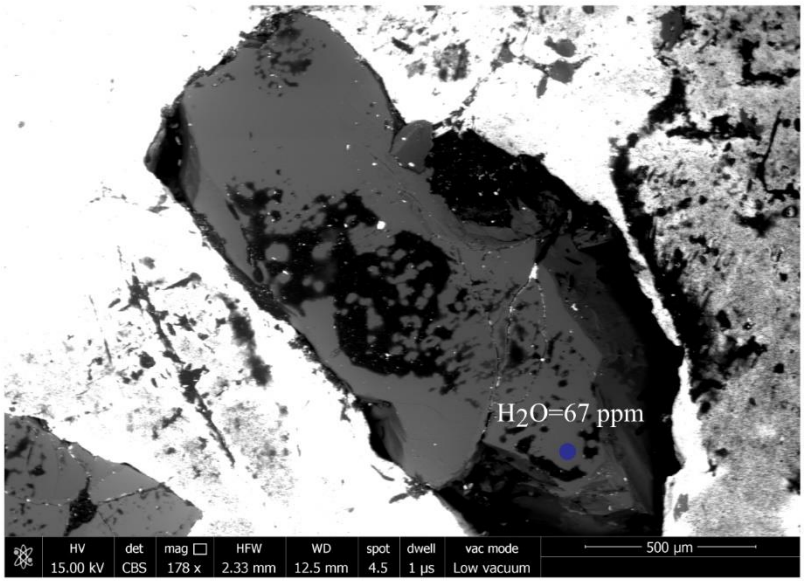

Sample 17MMSG02b, pyroxene 3

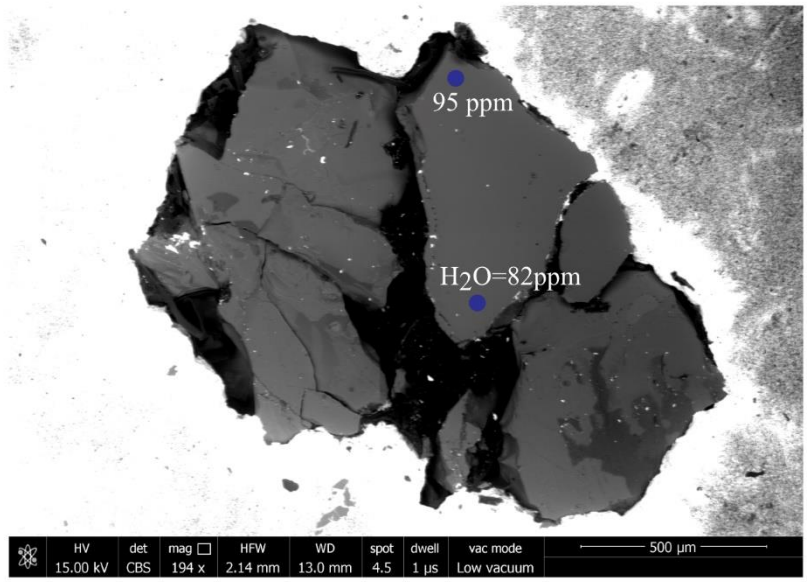

Sample 17MMSG02c, pyroxene 1

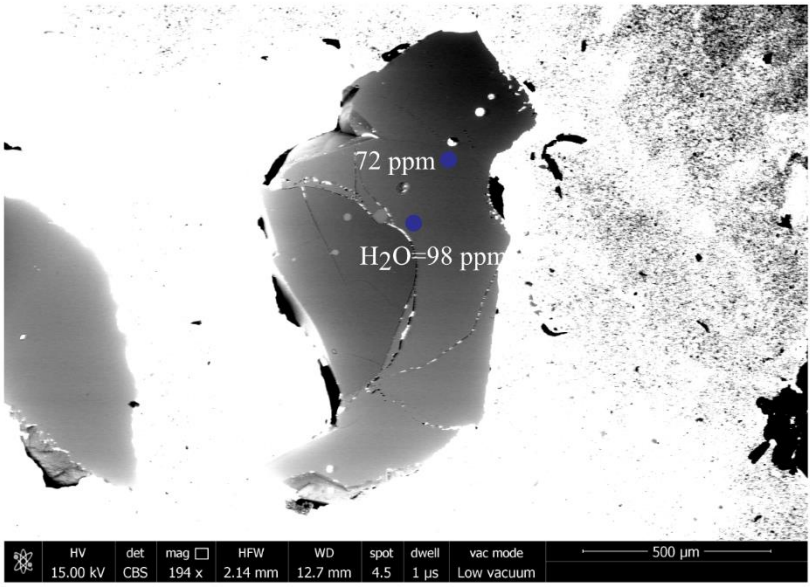

Sample 17MMSG02c, pyroxene 2

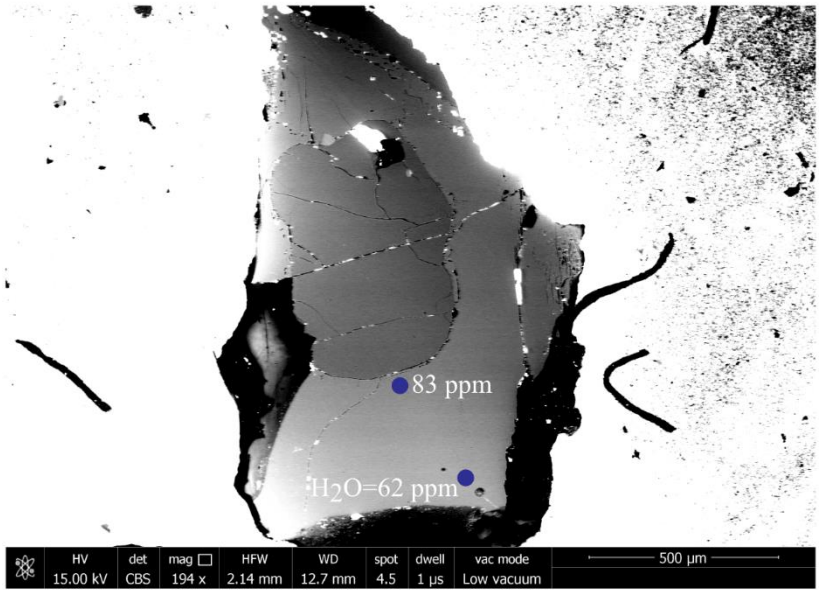

Sample 17MMSG03a, pyroxene 1 (ablation of nano inclusion may explain the anomalously high H_2O contents of one of the core analyses)

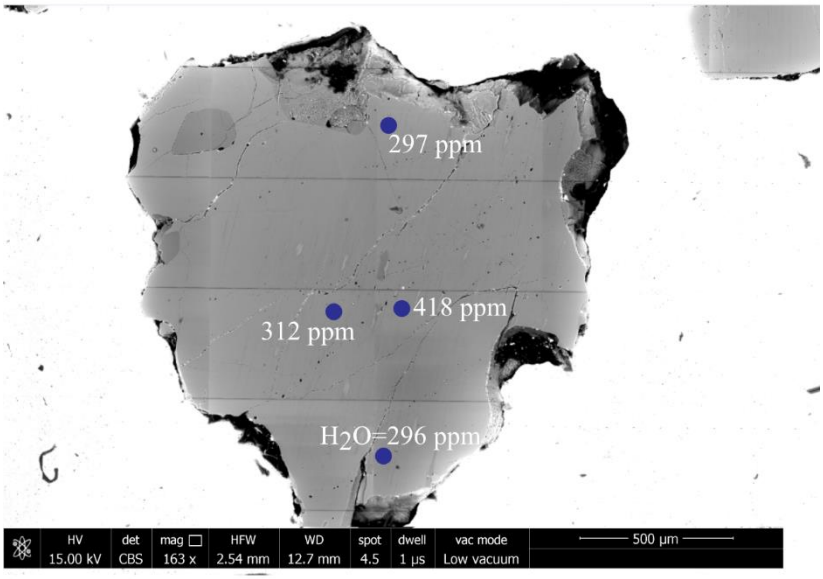

Sample 17MMSG03a, pyroxene 2 (gradient in H_2O contents across the crystal)

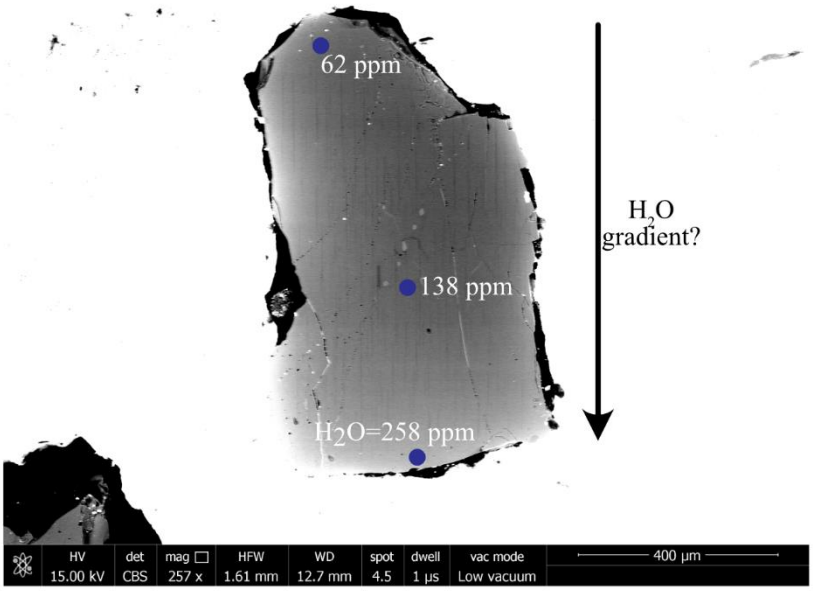

Sample 17MMSG03b, pyroxene 1

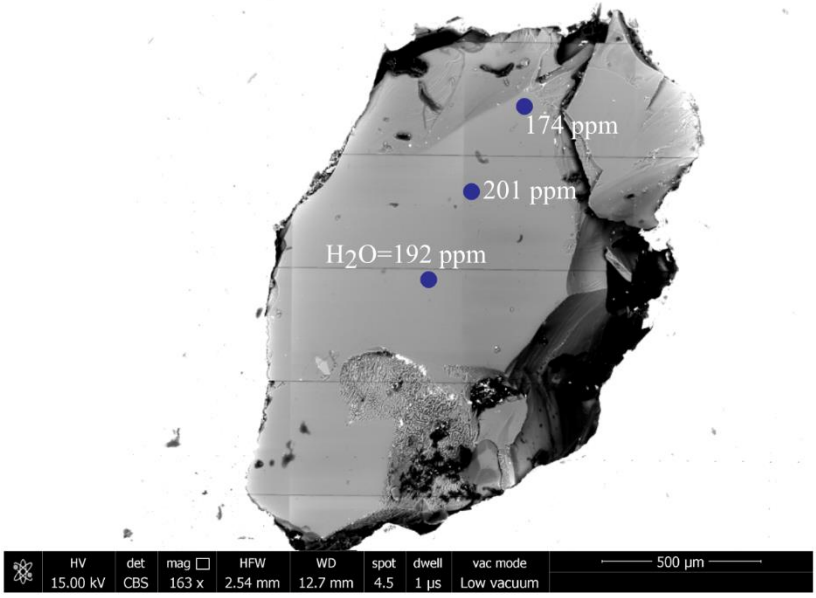

Sample 17MMSG03b, pyroxene 2

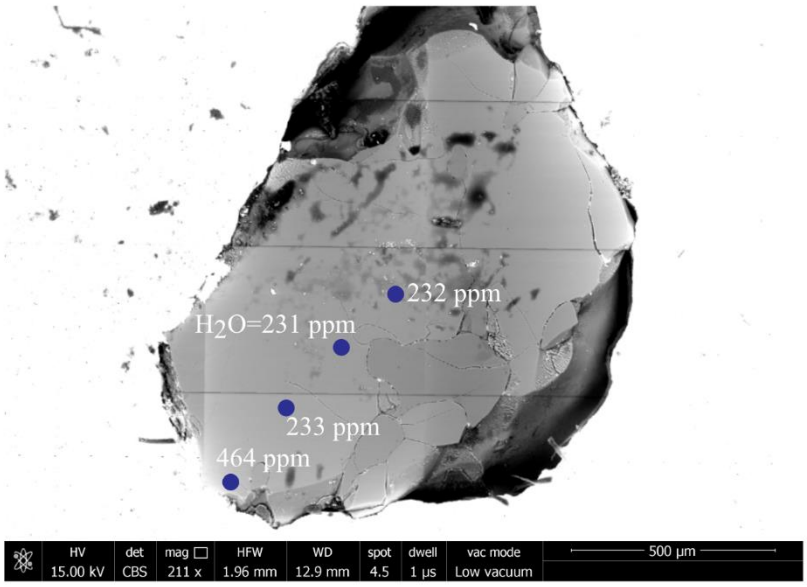

Sample 17MMSG04b, pyroxene 3

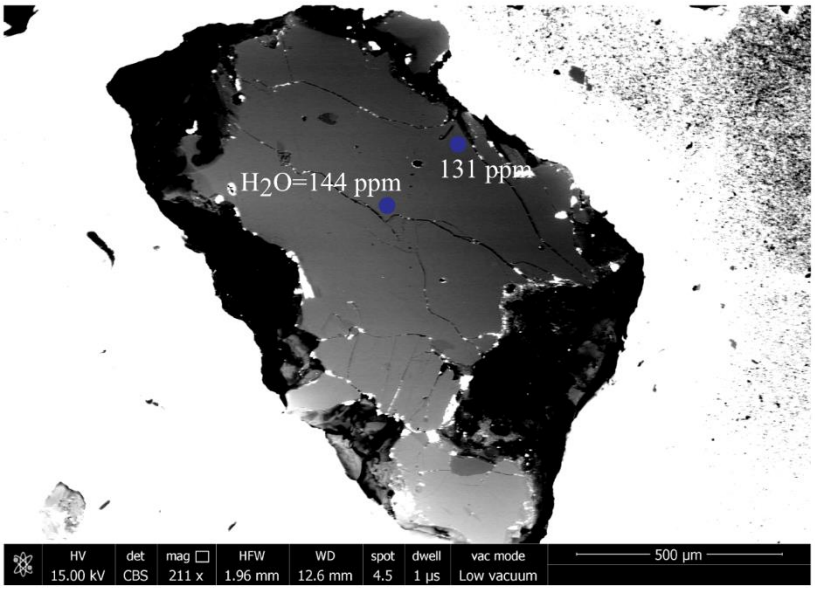

Sample 17MMSG04b, pyroxene 4

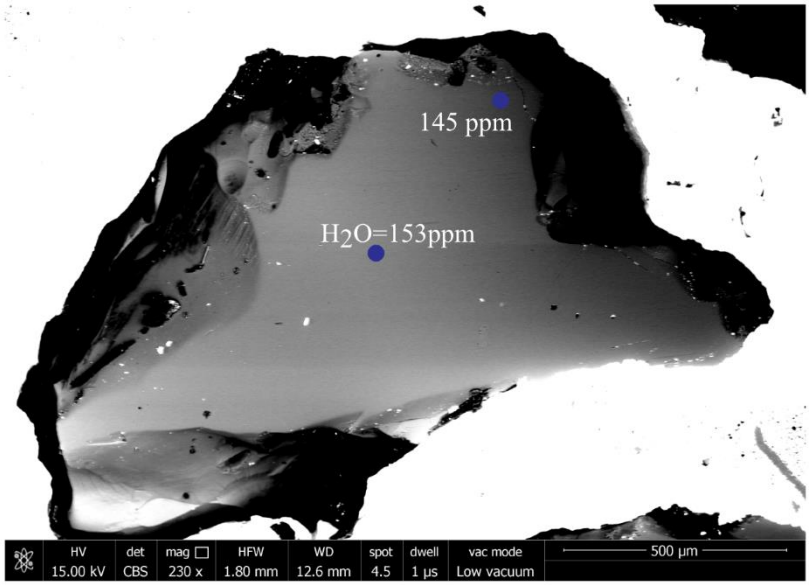

Sample 17MMSG04b, pyroxene 5

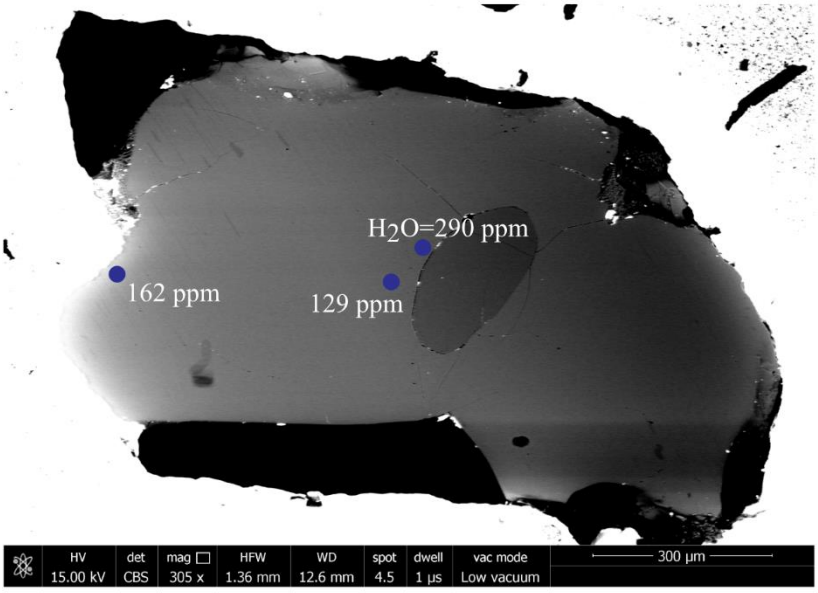

Sample 17MMSG04b, pyroxene 6

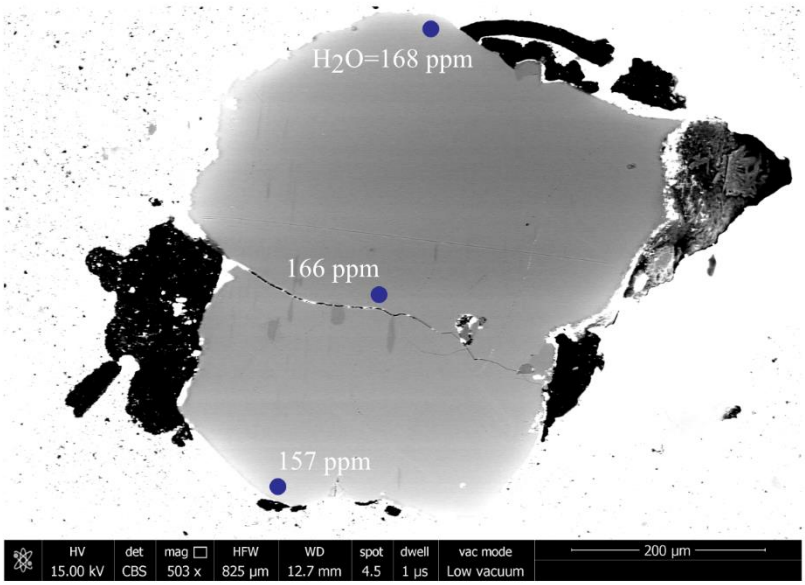

Sample 17MMSG04c, pyroxene 1

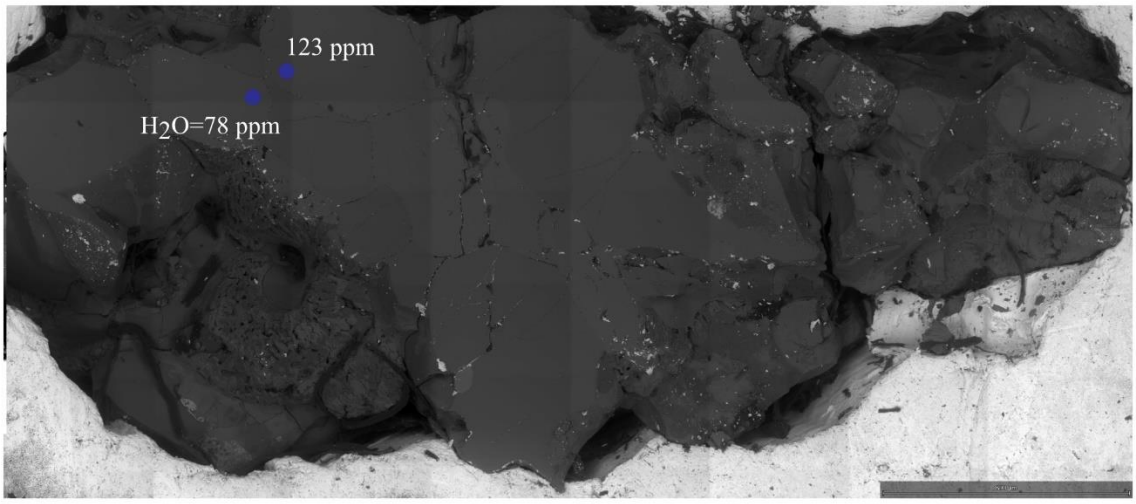

Sample 17MMSG04c, pyroxene 2

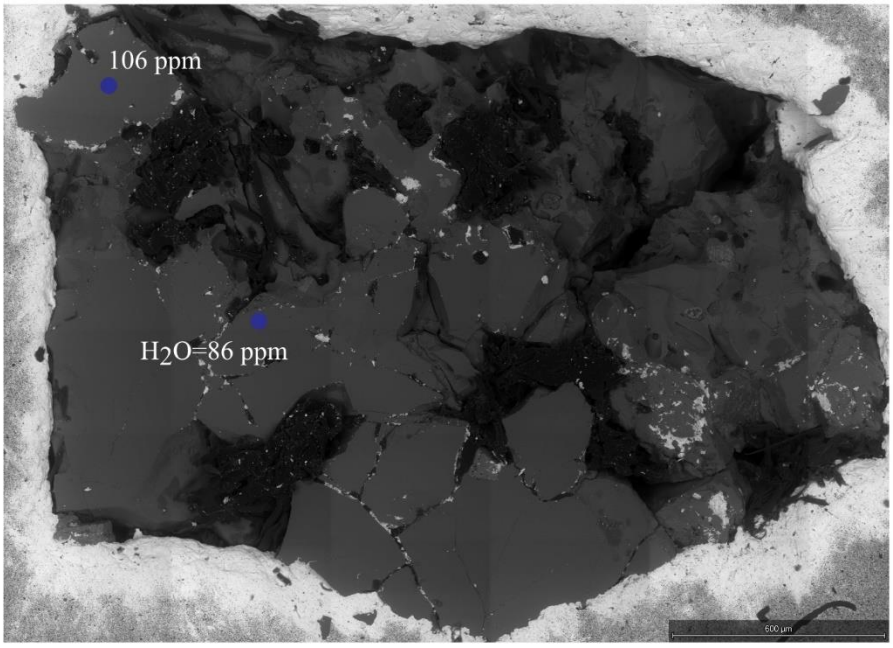

Sample 17MMSG04f, pyroxene 1

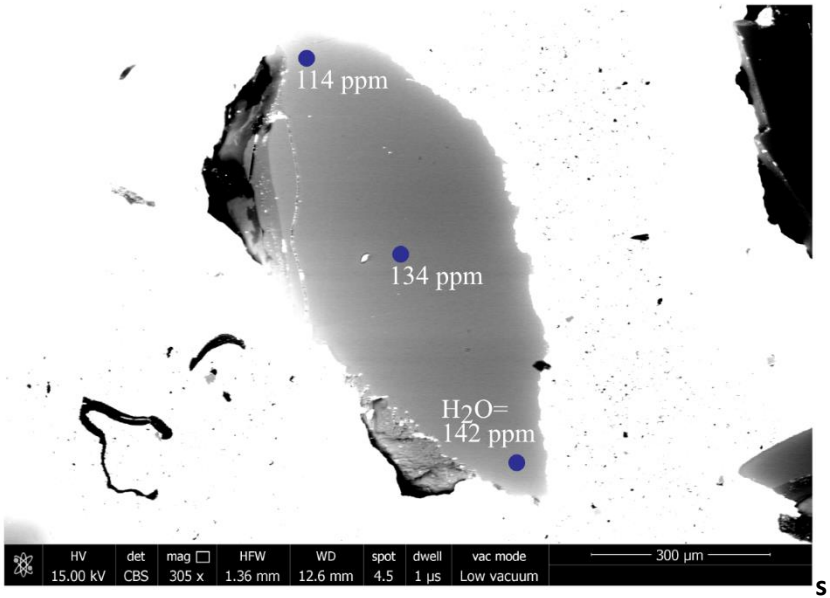

S

REFERENCES

Ghiorso, M.S., Gualda, G.A.R., 2015. An H2O–CO2 mixed fluid saturation model compatible with rhyolite-MELTS. Contrib. Mineral. Petrol. 169, 53. https://doi.org/10.1007/s00410-015-1141-8

Harpp, K., Geist, D., Koleszar, A.M., Christensen, B., Lyons, J., Sabga, M. and Rollins, N., 2014. The geology and geochemistry of Isla Floreana, Galápagos: a different type of late stage ocean island volcanism. *Galápagos Nat. Lab. Earth Sci. In: AGU Monogr*, *204*, pp.71-118.

Iacono-Marziano, G., Morizet, Y., Le Trong, E., Gaillard, F., 2012. New experimental data and semi-empirical parameterization of H2O–CO2 solubility in mafic melts. Geochim. Cosmochim. Acta 97, 1–23. https://doi.org/10.1016/j.gca.2012.08.035

Iacovino, K., Matthews, S., Wieser, P., Moore, G., Bégué, F., 2020. VESIcal Part I: An open-source thermodynamic model engine for mixed volatile (H_2O-CO_2) solubility in silicate melts (preprint). Earth Sciences. https://doi.org/10.31223/X5D606

Kumamoto, K.M., Warren, J.M. and Hauri, E.H., 2017. New SIMS reference materials for measuring water in upper mantle minerals. *American Mineralogist*, *102*(3), pp.537-547. https://doi.org/10.2138/am-2017-5863CCBYNCND

Matzen, A.K., Baker, M.B., Beckett, J.R. and Stolper, E.M., 2011. Fe–Mg partitioning between olivine and high-magnesian melts and the nature of Hawaiian parental liquids. *Journal of Petrology*, *52*(7-8), pp.1243-1263. https://doi.org/10.1093/petrology/egq089

Shishkina, T.A., Botcharnikov, R.E., Holtz, F., Almeev, R.R., Jazwa, A.M., Jakubiak, A.A., 2014. Compositional and pressure effects on the solubility of H2O and CO2 in mafic melts. Chem. Geol. 388, 112–129. https://doi.org/10.1016/j.chemgeo.2014.09.001

Shishkina, T.A., Botcharnikov, R.E., Holtz, F., Almeev, R.R. and Portnyagin, M.V., 2010. Solubility of H2O-and CO2-bearing fluids in tholeiitic basalts at pressures up to 500 MPa. *Chemical geology*, *277*(1-2), pp.115-125. https://doi.org/10.1016/j.chemgeo.2010.07.014

Witham, F., Blundy, J., Kohn, S.C., Lesne, P., Dixon, J., Churakov, S.V., Botcharnikov, R., 2012. SolEx: A model for mixed COHSCl-volatile solubilities and exsolved gas compositions in basalt. *Comput. Geosci.* 45, 87–97. https://doi.org/10.1016/j.cageo.2011.09.021

Zhang, Y., Ni, H., 2010. Diffusion of H, C, and O Components in Silicate Melts. *Rev. Mineral. Geochem*. 72, 171–225. https://doi.org/10.2138/rmg.2010.72.5

Zhang, Y., Ni, H., Chen, Y., 2010. Diffusion Data in Silicate Melts. *Rev. Mineral. Geochem.* 72, 311–408. https://doi.org/10.2138/rmg.2010.72.8